Threshold Effects in Neutron Elastic Scattering*

J. T. WELLS, A. B. TUCKER, AND W. E. MEYERHOF
Department of Physics, Stanford University, Stanford, California
(Received 8 April 1963)

In an attempt to observe the Wigner-cusp phenomenon in neutron elastic scattering near inelastic thresholds, we have measured the differential elastic and total cross sections of Li, Fe, Zr, Ba, and Ce near the threshold energy for exciting the first-excited states of the dominant isotopes of these elements. The energy region investigated extended approximately 300 keV on either side of threshold. Successful analysis of observed cusp phenomena can provide information on the spin and parity of excited states. In addition, the presence or absence of below-threshold effects in regions of neutron energy and atomic number where "energy-averaged" Wigner-cusp theory applies in principle can give an indication of the interaction mechanism, i.e., direct interaction or compound nucleus formation. The theory of Wigner cusps and "energy-averaged" Wigner cusps is supplemented in the present work by a consideration of slightly more general angular-momentum situations and by explicit cusp expressions for differential-elastic cross sections. Cusp predictions are given in terms of the coefficients for expansion of the cross sections into a series of Legendre polynomials. This form facilitates comparison of theory and experiment. Unusual features were observed at the inelastic thresholds in the elastic and total cross sections of Li and Fe. Here one expects to notice a below, as well as above, threshold effect characteristic of Wigner cusps. In these cases, however, the interpretation of the experimental results is not unambiguous—in Li because the predicted cusp effect is too small to be observable in the present experiment and in Fe because the resonance structure of the cross sections overshadows the expected cusp effect. A drop, commencing at inelastic thresholds, is observed in the elastic cross sections of Ce, Ba, and Zr. Analysis of this effect in terms of the theory of "energy-averaged" Wigner-cusps yields good agreement between theory and experiment.

INTRODUCTION

We have attempted to demonstrate the Wigner-cusp phenomenon[1] in neutron elastic scattering and total cross sections near the thresholds for excitation of the first-excited states of the dominant isotopes of Li, Fe, Zr, Ba, and Ce. Theoretical work (see, for example, Newton,[2] Baz,[3,4] Fonda,[5] and Meyerhof[6,7]) provides detailed predictions of possible cusp effects. The effects originate essentially in two fundamental physical principles: the conservation of incident flux, expressed in the theory as unitarity of the scattering matrix; and the uncertainty principle of Heisenberg, expressed in the theory as analyticity of the scattering matrix. The magnitude and shape of cusp anomalies can yield information useful in scattering analysis and in establishing spins and parities of excited states.

Cusp anomalies have been seen in proton elastic and inelastic scattering near thresholds for (p,n) reactions.[8–10] The theory shows that one essential requirement for a sharp cusp is that Coulomb effects be absent from that reaction channel which provides the threshold.[11] Any reaction with outgoing neutrons, such as (p,n) (d,n) (α,n) (n,n'), satisfies this requirement.

An advantage of studying Wigner cusps in elastic neutron, rather than elastic proton scattering, for example, is the easier analysis caused by the absence of Coulomb effects in the *incoming* channel. After estimating possible cusp magnitudes, we concluded that the effects of inelastic neutron scattering reactions on elastic neutron scattering might be quite noticeable for selected cases. We hoped thereby to find a method for spin assignment of excited states and to elucidate interaction mechanisms between nuclei and neutrons of few MeV energy.

Previous articles on the theory of Wigner cusp phenomena have generally emphasized the simple spin cases (e.g., spinless particles); also, the results are not always given in a form readily compared with experiment. We would like to supplement the previous results by considering slightly more general spin and angular momentum configurations. Our results provide a convenient form for experimental comparisons and include differential cross-section expressions. In addition, the form of the results for pure Wigner-cusp effects is particularly suitable for subsequent deduction of "energy-averaged" cusp expressions.[6]

THEORY OF WIGNER CUSPS

Pure Wigner-Cusp Theory

The effect of reactions of the type $X(n,n')X^*$ on neutron differential elastic and total cross sections near threshold energies is easily computed. Blatt and

* This work was supported in part by the U. S. Army Research Office (Durham), the joint program of the Office of Naval Research and the U. S. Atomic Energy Commission, and the National Science Foundation.

[1] E. P. Wigner, Phys. Rev. **73**, 1002 (1948).
[2] R. G. Newton, Phys. Rev. **114**, 1611 (1959).
[3] A. I. Baz, Zh. Eksperim. i Teor. Fiz. **33**, 923 (1958) [translation: Soviet Phys.—JETP **6**, 709 (1957)].
[4] A. I. Baz, L. D. Puzikor, and Ya. A. Smorodinskiĭ, Zh. Eksperim. i Teor. Fiz. **42**, 1249 (1962) [translation: Soviet Phys.—JETP **15**, 865 (1962)].
[5] L. Fonda, Nuovo Cimento **20**, 116 (1961).
[6] W. E. Meyerhof, Phys. Rev. **128**, 2312 (1962).
[7] W. E. Meyerhof, Phys. Rev. **129**, 692 (1963).
[8] P. R. Malmberg, Phys. Rev. **101**, 114 (1955).
[9] N. Jarmie and R. C. Allen, Phys. Rev. **114**, 176 (1955).
[10] H. W. Newson, R. M. Williamson, K. W. Jones, J. H. Gibbons, and H. Marshak, Phys. Rev. **108**, 1294 (1957).
[11] G. Breit, Phys. Rev. **107**, 1612 (1957).

Biedenharn[12] have derived the necessary general expressions for cross sections. In applying these formulas we assume that *elastic* scattering with change of orbital angular momentum l may be neglected. Because of the parity rule requiring $\Delta l=0, 2, 4, \cdots$, elastic scattering with change of l turns out to be an unimportant phenomenon in most situations,[13] especially those of interest here. Also, to preserve clarity in the presentation, we will restrict our derivation to situations in which channel spin, s is separately conserved.

The following equations are numbered (3.16), (4.5), and (4.6) in Ref. 12. We have specialized them to elastic scattering with no change of α, l, s, or i. Accordingly, the differential elastic scattering cross section is given by

$$d\sigma_{\alpha;\alpha}=\sum_{s=|I-i|}^{I+i}\{(2s+1)/[(2I+1)(2i+1)]\}d\sigma_{\alpha s;\alpha s}, \quad (1)$$

where

$$d\sigma_{\alpha s;\alpha s}=[\lambda\!\!\!^{-}_{\alpha}{}^2/(2s+1)]\sum_{L=0}^{\infty}B_L(\alpha s;\alpha s)P_L(\cos\theta)d\Omega, \quad (2)$$

$$B_L(\alpha s;\alpha s)=(\tfrac{1}{4})\sum_{J_1}\sum_{J_2}\sum_{l_1}\sum_{l_2}Z^2(l_1J_1l_2J_2,sL)\times\mathrm{Re}[(1-S_{\alpha sl_1;\alpha sl_1}{}^{J_1})^*(1-S_{\alpha sl_2;\alpha sl_2}{}^{J_2})], \quad (3)$$

and where α refers to the type of incident particle and the state of the struck nucleus; $\lambda\!\!\!^{-}_{\alpha}$ is $(2\pi)^{-1}\times$the reduced de Broglie wavelength of the incident neutron in the center-of-mass system; s, I, and i are channel, target, and projectile spins, respectively; and l, J are orbital and total angular momentum, respectively. Subscripts 1 and 2 are dummy indices for use in summation. All sums are unrestricted, except that, in practice, only one such sum, for example, J_1, runs to infinity, because of the vanishing of Z coefficients. Re stands for real part of the bracketed expression. $S_{\alpha sl;\alpha sl}{}^{J}$ is the S-matrix element for elastic scattering with l and s conserved.

$$Z(l_1J_1l_2J_2,sL)=(2l_1+1)^{1/2}(2l_2+1)^{1/2}(2J_1+1)^{1/2}(2J_2+1)^{1/2}\times W(l_1J_1l_2J_2,sL)(l_1l_200\,|\,l_1l_2L0),$$

where W is the Racah coefficient.[14] Tables of Z are available.[15] The properties of W are discussed by Biedenharn, Blatt, and Rose.[16] We have omitted a phase factor from Z as defined in Ref. 16, in accordance with a correction given by Huby.[17] The energy dependence of the elastic cross section is contained in the elements of **S**.

Among the inelastic reactions which can proceed from a given incident partial wave, we consider only the one with lowest threshold energy. However, an excitation of a higher excited state is not excluded as long as its threshold has the lowest energy of those reactions which may proceed from a particular incident partial wave. Baz[3] showed that the procedure for including higher inelastic thresholds of the same dominant partial wave is straightforward in principle, although much more complicated. Also, weak inelastic processes (e.g., neutron capture) occurring at lower energy than the threshold energy of interest are neglected.

In addition, we restrict the energy region in which the derivation is valid to that in which the reaction is dominated by a single incident partial wave. In practice, such an energy region is usually sufficiently large to be of experimental interest. For example, an incident d wave contributes more than 90% of the cross section over an energy interval of 150 keV above threshold for inelastic neutron scattering leading to the 2^+ first excited state of Ce^{140}.[18] One can explain this in terms of the optical model by noting that Ce has a large transmission coefficient for (low energy) outgoing s-wave neutrons,[19] and that sufficiently close to threshold, inelastic neutron scattering is always dominated by that incident partial wave which is associated (through angular momentum conservation) with an outgoing s wave.

Finally, to further simplify the presentation, but not as an essential limitation on the theory, we will only consider reactions dominated by outgoing s waves. The complete theory in this respect shows that reactions dominated near threshold by outgoing waves of orbital angular momentum l_0, greater than zero, produce cusp effects in the (l_0)th derivative of the elastic cross section.[11] Therefore, these cases have less experimental interest. With one exception, this restriction is not essential since we measured threshold effects of reactions with outgoing s waves. The exceptional case is the reaction $Zr^{90}(n,n')Zr^{90*}$ (1.75 MeV) which Tucker *et al.* have found dominated by outgoing p waves already at about 30 keV above threshold.[20] The necessary modifications to the theory in the case of Zr^{90} will be obvious.

Under the above assumptions, the reaction cross section

$$\sigma_r=\sigma_{rl'}=\sum_{s'=|I-i|}^{I+i}\frac{2s'+1}{(2I+1)(2i+1)}\sum_{J'=|l'-s'|}^{l'+s'}\sigma_{rl's'}{}^{J'} \quad (4)$$

[12] J. M. Blatt and L. C. Biedenharn, Rev. Mod. Phys. **24**, 258 (1952).
[13] J. M. Blatt and V. F. Weisskopf, *Theoretical Nuclear Physics* (John Wiley & Sons, Inc., New York, 1952), Chap. 8, Sec. 10.
[14] G. Racah, Phys. Rev. **61**, 186 (1942); **62**, 438 (1942).
[15] L. C. Biedenharn, Oak Ridge National Laboratory Report ORNL-1501, 1953 (unpublished).
[16] L. C. Biedenharn, J. M. Blatt, and M. Rose, Rev. Mod. Phys. **24**, 248 (1952).
[17] R. Huby, Proc. Phys. Soc. (London) **67**, 1103 (1954).
[18] P. A. Moldauer (private communication).
[19] H. Feshbach, in *Nuclear Spectroscopy*, edited by F. Ajzenberg-Selove (Academic Press Inc., New York, 1960), Part B, Chap. 6. D, p. 1058.
[20] A. B. Tucker, J. T. Wells, and E. W. Meyerhof (to be published).

may be described by its partial-reaction cross sections

$$\sigma_{r\alpha l's'J'}=\pi\lambda\!\!\!^{-}_{\alpha}{}^{2}g_{s'J'}(1-|S_{\alpha l's';\alpha l's'J'}|^2), \quad (5)$$

where primes identify the particular channel quantities which couple to l', the dominant incident partial wave, and $g_{s'J'}=(2J'+1)/(2s'+1)$. Henceforth, we drop the subscript α because we always consider a neutron incident upon the ground state of a target nucleus.

In Appendix A the unitary and analytic properties of the **S** matrix have been used to obtain an expression for elastic cross sections in the vicinity of the reaction threshold. It is also shown that the Wigner-cusp term $\Delta d\sigma$ can be defined by the set of equations

$$d\sigma=d\sigma^0+\Delta d\sigma, \quad (6)$$

where superscript "0" means "without reaction effects," and where

$$\Delta d\sigma=\sum_{s'=|I-i|}^{I+i}[(2s'+1)/(2I+1)(2i+1)]\Delta d\sigma_{s';s'}, \quad (7)$$

$$\Delta d\sigma_{s';s'}=[\lambda\!\!\!^{-2}/(2s'+1)]\sum_{L=0}^{\infty}\Delta B_L(s';s')P_L(\cos\theta)d\Omega, \quad (8)$$

and

$$\Delta B_L(s',s')=-(\tfrac{1}{4})\sum_J\sum_l\sum_{J'}Z^2(lJl'J',s'L)(\pi\lambda\!\!\!^{-2}g_{s'J'})^{-1}$$

$$\times\sigma_{rl's'J'}2\sin\delta_{ls'}{}^{J}\begin{Bmatrix}\sin(2\delta_{l's'J'}-\delta_{ls'J})\\ \mathfrak{F}\cos(2\delta_{l's'J'}-\delta_{ls'J})\end{Bmatrix}, \quad (9)$$

where $2\delta_{ls}{}^{J}$ is defined in Appendix A to be the phase of $S_{ls;ls}{}^{0J}$ and $\mathfrak{F}$ is a theoretically derived correction to the magnitude of the below-threshold effect. The upper and lower parts of the bracket refer to above and below-threshold effects, respectively.

Within the limitations imposed during the derivation, Eqs. (6), (7), (8), and (9) describe the expected Wigner-cusp effects. The cusp effect is completely contained in the coefficients B_L in Eq. (2); that is, $B_L=B_L{}^0+\Delta B_L$, where ΔB_L is given by Eq. (9). Since it is frequent practice (cf. Ref. 21) to analyze neutron scattering data in terms of the B_L coefficients, the utility of Eq. (9) for cusp interpretation is clear. Should a cusp effect be found in only one or two of several experimental B_L coefficients then the properties of the Z coefficients severely restrict the participating partial waves.

We reiterate that the cusp predictions, Eqs. (7) to (9) are not generally valid if scattering is possible which conserves energy but not channel spin, because most detection systems are only energy-selective. In such cases, the threshold reaction is coupled (via unitarity of the S matrix) to other off-diagonal (different initial- and final-state channel spin) elements, as well as a diagonal element ("pure" elastic scattering) of the S matrix (see Eq. 5). An additional sum over final-state channel spins is required in Eq. (1). As a result additional cusp terms appear in Eq. (7). Unless polarization is also measured, comparisons of theory and experiment are ambiguous in such cases. None of the present experimental results required this extension.

The expected Wigner cusp in total cross sections (σ_T) is easily obtained if we recall that, by assumption, the interaction in the (l')th incident channel is purely elastic below threshold.

$$\sigma_T=\int(d\sigma/d\Omega)d\Omega+\sigma_{rl'}\begin{Bmatrix}1\\0\end{Bmatrix}$$

$$=\sigma_T{}^0+\left[\int(\Delta d\sigma/d\Omega)d\Omega+\sigma_{rl'}\begin{Bmatrix}1\\0\end{Bmatrix}\right]$$

$$\equiv\sigma_T{}^0+\Delta\sigma_T, \quad (10)$$

where $\sigma_T{}^0$ is the total cross section "without reaction effects."

In Appendix A it is shown that

$$\Delta\sigma_T=\sum_{s'=|I-i|}^{I+i}\frac{(2s'+1)}{(2I+1)(2i+1)}$$

$$\times\sum_{J'=|l'-s'|}^{l'+s'}\sigma_{rl's'J'}\begin{Bmatrix}\cos2\delta_{l's'J'}\\ -\mathfrak{F}\sin2\delta_{l's'J'}\end{Bmatrix}. \quad (11)$$

Equation (11) combined with Eq. (10), is the general expression for Wigner-cusp effect in the total cross section, within the limitations imposed by the derivation.

We now extract the special case of spinless particles from these expressions, for comparison with other work. If all spins are zero, including that of the residual nucleus in the reaction, then Eq. (9) becomes

$$\Delta B_L(0;0)=-(\tfrac{1}{4})\sum_l Z^2(ll00,0L)(\pi\lambda\!\!\!^{-2})^{-1}$$

$$\times2\sin\delta_l\,\sigma_r\begin{Bmatrix}\sin(2\delta_0-\delta_l)\\ \mathfrak{F}\cos(2\delta_0-\delta_l)\end{Bmatrix},$$

where $\delta_l\equiv\delta_{l0}{}^{l}$ and $\sigma_r\equiv\sigma_{r00}{}^{0}$. Since $Z(ll00,0L)=\delta_{lL}{}^{K}$, where $\delta_{lL}{}^{K}$ is a Kronecker delta, the sum in ΔB_L is reduced to one term, and using Eqs. (7) and (8) we obtain

$$\Delta d\sigma=-(\sigma_r/4\pi)\sum_{l=0}^{\infty}2\sin\delta_l\begin{Bmatrix}\sin(2\delta_0-\delta_l)\\ \mathfrak{F}\cos(2\delta_0-\delta_l)\end{Bmatrix}P_l d\Omega.$$

This expression can be written as

$$\Delta d\sigma=2\,\mathrm{Re}\Bigg(\left[\tfrac{1}{2}i\lambda\!\!\!^{-}\sum_{l=0}^{\infty}(1-\exp2i\delta_l)P_l\right]^*$$

$$\times(\sigma_r/2\pi\lambda\!\!\!^{-})^{\frac{1}{2}}(\exp2i\delta_0)\begin{Bmatrix}1\\ i\mathfrak{F}\end{Bmatrix}\Bigg)d\Omega$$

$$=2\,\mathrm{Re}\left[(1/\lambda\!\!\!^{-})f^*(\theta)\tfrac{1}{2}\sigma_r(\exp2i\delta_0)\begin{Bmatrix}1\\ i\mathfrak{F}\end{Bmatrix}\right]d\Omega, \quad (12)$$

where $f^*(\theta)$ is the complex conjugate of the scattering amplitude, with its explicit form evident by comparison with the preceding line.

This is just the cusp term obtained by Baz,[4] for the case of spinless particles (if δ_0 is assumed to vary slowly with incident energy across threshold). Baz emphasized the explicit appearance of the scattering amplitude, suggesting that there is additional theoretical significance in cusp data beyond cross-section measurements (squared amplitudes) that are usually made. We would like to caution that most cases in practice involve nonzero spins; consequently, scattering amplitudes, in general, are azimuth angle (φ)-dependent. Comparison of theoretical cusp effects with experiment may be undertaken if the theroetical expressions have been averaged and summed over magnetic quantum numbers. This is essentially what we have accomplished, and, in general, little vestige of complete amplitude forms is found in the resulting expressions.

On the other hand, it is useful to see from Eq. (12) that one can estimate expected above-threshold Wigner cusp magnitudes from the expression

$$|\Delta d\sigma/d\Omega| \approx \sigma_r (d\sigma^0/d\Omega)^{1/2}/\lambda\,,$$

the remainder of the cusp expression being of order unity. The expected percentage cups effect (above threshold) is inversely proportional to $(d\sigma^0/d\Omega)^{1/2}$ and exploratory experiments might well be undertaken at angles where the cross section is least.

The spinless-particle result for total cross sections is a trivial reduction of Eqs. (10) and (11) to

$$\sigma_T = \sigma_T{}^0 + \sigma_r \begin{Bmatrix} \cos 2\delta_0 \\ -\mathfrak{F} \sin 2\delta_0 \end{Bmatrix}. \tag{13}$$

This result is in agreement with those of others (if $\mathfrak{F} \to 1$).[2,3,6]

Theory of "Energy-Averaged" Wigner Cusps

If the measured cross sections are effectively energy averages of the actual detailed cross sections, containing closely spaced or overlapping resonance structure, the energy average of Wigner-cusp expressions leads to a predicted threshold effect which we shall call an "energy-averaged" Wigner cusp.[6,7]

Noting that the energy dependence of differential elastic cusp effects is contained in $\Delta B_L(s';s')$ [see Eq. (9)] we can isolate the energy-dependent quantities,

$$\left\langle \sigma_{rl's'}{}^{J'} 2 \sin\delta_{ls'}{}^{J} \begin{Bmatrix} \sin(2\delta_{l's'}{}^{J'} - \delta_{ls'}{}^{J}) \\ \mathfrak{F} \cos(2\delta_{l's'}{}^{J'} - \delta_{ls'}{}^{J}) \end{Bmatrix} \right\rangle. \tag{14}$$

Brackets, $\langle\ \rangle$, imply that an energy average is to be taken over an interval containing many resonances. The phases $\delta_{ls'}{}^{J}$ and $\delta_{l's'}{}^{J'}$ are rapidly varying with energy over the averaging interval and we will assume they are uncorrelated for $J \neq J'$ and/or $l \neq l'$.

Using R-matrix theory and applying the random sign assumption to certain value quantities γ_λ, which will be discussed, it can be shown[7] that

$$\left\langle \sigma_{rl's'}{}^{J'} \begin{Bmatrix} 2\sin^2\delta_{l's'}{}^{J'} \\ \mathfrak{F} \sin 2\delta_{l's'}{}^{J'} \end{Bmatrix} \right\rangle \approx \begin{Bmatrix} \langle \sigma_{rl's'}{}^{J'} \rangle \\ 0 \end{Bmatrix}, \tag{15}$$

and

$$\left\langle \sigma_{rl's'}{}^{J'} \begin{Bmatrix} -\cos 2\delta_{l's'}{}^{J'} \\ \mathfrak{F} \sin 2\delta_{l's'}{}^{J'} \end{Bmatrix} \right\rangle \approx \begin{Bmatrix} 0 \\ 0 \end{Bmatrix}. \tag{16}$$

The value quantities γ_λ mentioned above were introduced by Wigner and Eisenbud[21] to parametrize the terms of the R matrix, each of which has a resonance denominator. Thus, these quantities correspond to resonances and could be indexed in our notation by $\gamma_{\lambda ls}{}^{J}$, where λ specifies a particular resonance of the set associated with angular momenta J, l and spin s. The random-sign assumption leading to Eqs. (15) and (16) is made for value quantities of different index J, l, or s, but is not justified for relating value quantities of the same J, l, and s, but different λ, i.e., different resonances initiated by the same partial wave may have correlated phases. In particular, the reaction cross section appearing in the averaging brackets in Eqs. (15) and (16) proceeds through resonances correlated in phase to the remaining expression in the bracket, and it is surprising that the simple results were obtained.

In Appendix B, we show how Eqs. (15) and (16) can be applied to expression (14) to give the result

$$\left\langle \sigma_{rl's'}{}^{J'} 2 \sin\delta_{ls'}{}^{J} \begin{Bmatrix} \sin(2\delta_{l's'}{}^{J'} - \delta_{ls'}{}^{J}) \\ \mathfrak{F} \cos(2\delta_{l's'}{}^{J'} - \delta_{ls'}{}^{J}) \end{Bmatrix} \right\rangle \approx \begin{Bmatrix} \langle \sigma_{rl's'}{}^{J'} \rangle \\ 0 \end{Bmatrix} \delta_{ll'}{}^{K} \delta_{JJ'}{}^{K}, \tag{17}$$

where δ^K is a Kronecker delta.

Part of the proof of Eqs. (15) and (16), which led to Eq. (17), depends upon a cancellation of path integrals used in the energy averaging process, which will be complete only if normally slowing varying quantities remain slowly varying throughout the averaging interval. For the case of outgoing s waves in the reaction channel, one of these quantities (the logarithmic derivative of the outgoing wave function) does not vary slowly right at reaction threshold. In essence, this difficulty is just the result of rediscovering pure Wigner-cusp phenomena as one formally approaches very close to threshold in the averaging process. This means that the derivation of Eqs. (15) and (16) is not strictly valid arbitrarily close to threshold. The actual experimental result would depend on the exact energy distribution of the beam.[22] As long as the energy distribution of the beam does not overlap the threshold, the results,

[21] E. P. Wigner and L. Eisenbud, Phys. Rev. **72**, 29 (1947).
[22] P. A. Moldauer, Phys. Rev. **129**, 754 (1963).

i.e., Eqs. (15) and (16) and consequently Eq. (17), will be applicable.

After justifying Eq. (17) we have completed the derivation of "energy-averaged" cusp expressions. Recalling Eq. (9), which contains expression (14), and using Eq. (17), we obtain

$$\langle \Delta B_L(s';s') \rangle = -(\tfrac{1}{4}) \sum_{J'} Z^2(l'J'l'J';s'L) \times (\pi \lambda\!\!\!^{-2} g_{s'}{}^{J'})^{-1} \begin{Bmatrix} \langle \sigma_{rl's'}{}^{J'} \rangle \\ 0 \end{Bmatrix}. \quad (18)$$

The sums over l and J have vanished due to the occurrence of $\delta_{ll'}{}^{K}$ and $\delta_{JJ'}{}^{K}$ in Eq. (17). The "energy-averaged" differential cross-section cusp term is obtained by substituting Eq. (18) in Eqs. (6) to (8).

Substitition of relation (16) in Eq. (11) gives the previously derived[7] result for the total cross section,

$$\langle \Delta \sigma_T \rangle = \begin{Bmatrix} 0 \\ 0 \end{Bmatrix}. \quad (19)$$

That is, under the random sign assumption, there is no "energy-averaged" cusp in the total cross section.[7]

We give the results for a special case of Eq. (7), with Eq. (18) substituted, of particular interest in comparison with the present experimental data, where the incident particle is a neutron, the target nucleus is even-even, and one incident wave l' dominates the reaction.

$$I=0, \quad i=\tfrac{1}{2}, \quad J'=l'\pm\tfrac{1}{2},$$

$$\langle \Delta d\sigma \rangle = -(\langle \sigma_{rl'} \rangle/4\pi) \sum_{J'=|l'-\frac{1}{2}|}^{l'+\frac{1}{2}} R_{J'} \times \sum_L [Z^2(l'J'l'J',\tfrac{1}{2}L)/(2J'+1)] P_L \begin{Bmatrix} 1 \\ 0 \end{Bmatrix} d\Omega, \quad (20)$$

where $R_{J'}=\langle \sigma_{rl'}{}^{J'} \rangle / \langle \sigma_{rl'} \rangle$.

Although not immediately obvious, Eq. (20) is identical to Eq. (16′) in Ref. 6. To compare, one must identify

$$R_{l'+\frac{1}{2}}=(l'+1)/(l'+1+l'\bar{r}) \quad \text{and} \quad R_{l'-\frac{1}{2}}=l'\bar{r}/(l'+1+l'\bar{r}),$$

where $\bar{r}$ is defined and used in Ref. 6.

It turns out that the cusp prediction, Eq. (20), is relatively insensitive to the ratio $R_{J'}$. (Recall that $R_{J'}$ was defined as the fraction of the reaction probability which originates from compound resonances of a particular J', for example, $l'+\frac{1}{2}$.) We make the reasonable choice $R_{J'}=\frac{1}{2}(2J'+1)/(2l'+1)$ (or $\bar{r}=1$) which is the same as the fraction of the total number of incident states of the (l')th partial wave which have total angular momentum J'. With this choice of $R_{J'}$, Eq. (20) becomes, e.g., for $l'=2$

$$\langle \Delta d\sigma(l'=2) \rangle = -(\langle \sigma_{rl'=2} \rangle/4\pi) \begin{Bmatrix} 1 \\ 0 \end{Bmatrix} [1+(38/35)P_2(\cos\theta) + (18/35)P_4(\cos\theta)] d\Omega. \quad (21)$$

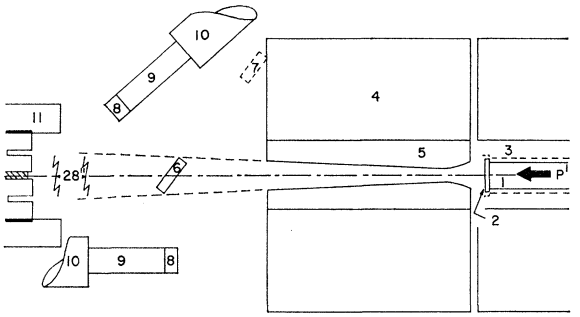

FIG. 1. Experimental arrangement: (1) Tritium-loaded target; (2) air-water spray coolant; (3) eccentric wobble for additional cooling effect; (4) paraffin shielding (loaded with Li_2CO_3); (5) paraffin (Li_2CO_3 loaded) rectangular conical collimator; (6) scatterer in "In Beam" position; (7) scatterer in "Out" position; (8) anthracene or stilbene crystal (a right circular cylinder, 2-in. diam × 1 in. long); (9) 6810A RCA photomultiplier tube; (10) preamplifier (linear and gamma-suppression outputs); (11) long counter in monitor position.

We note that in "energy-averaged" Wigner-cusp expressions no below-threshold effect is predicted. Since those complications in pure Wigner-cusp theory, which stem from outgoing-reaction channels with $l_0 \neq 0$, occur only in below-threshold cusp predictions,[7] in regions of mass number and energy where "energy-averaged" theory applies it is not necessary to specify the outgoing-reaction channel. In particular, outgoing p-wave dominance of the reaction in the Zr^{90} experiment, mentioned earlier, causes no difficulty in analysis. Determination of the dominant *incident* partial wave in the reaction and in Eq. (18) suffices.

EXPERIMENTAL METHOD

Differential Elastic Cross Section Measurements

Neutrons were produced by the $T(p,n)$ reaction, using tritium-loaded zirconium and titanium targets and the proton beam from a High Voltage Engineering Company 3-MeV Van de Graaff generator. Various tritium targets of 10- to 70-keV thickness at 1.02-MeV proton energy (as determined by the yield rise at threshold) were used. An eccentric circular motion was imposed upon the tritium target, causing the proton beam to strike a ring-shaped area. This technique minimized target-heating difficulties and averaged over nonuniform tritium deposition in the target.

The neutron beam was collimated by a rectangular conical opening in Li_2CO_3-loaded paraffin source shielding 18-in. thick. The geometry and shielding of the experiment are shown in Fig. 1. The collimation angle was such that the energy spread in the neutron beam due to $T(p,n)$ kinematics was approximately 4 keV. A standard long counter[23] placed at 0° with respect to the beam was used to monitor the neutron yield.

The neutron beam was allowed to strike the scatterer,

[23] A. O. Hanson and J. L. McKibben, Phys. Rev. **97**, 1205 (1955).

TABLE I. Description of scatterers.

Material	Dimensions (in.)	Angle between slab and beam (deg)
Scatterers used in $d\sigma/d\Omega$ measurements		
Cerium (a)	4.0 ×3.0 ×0.63	50
(b)	3.25×2.75×0.19	50
Barium	4.0 ×3.0 ×1.19	45
Zirconium	4.0 ×1.5 ×0.56	50
Iron	4.0 ×2.5 ×0.52	50
Lithium	3.05 diam ×4.4 high	cylinder
Samples used in σ_T (transmission) measurements		
Cerium	1.0 ×1.25×0.935 long[a]	
Barium	1.0 diam ×1.87 long[a]	
Iron	1.0 ×1.13×0.97 long[a]	

[a] The "long" dimension was parallel to the beam axis.

which was made slightly smaller than the collimator aperture, at about 10 in. from the collimator. The scatterers were in the shape of a slab, oriented with their normals parallel to the floor and at 40° to the incident beam direction, except for the lithium scatterer which was a right-circular cylinder oriented vertically. The scatterers are described in detail in Table I. Scatterer thicknesses were between $\frac{1}{5}$ and $\frac{5}{8}$ neutron mean free paths at the energies of experimental interest. These rather thick scatterers were necessary to obtain sufficient counting rates. Scattered neutrons were detected at two angles by organic scintillation crystals (2-in.-diam × 1-in.-long anthracene and 2-in.-diam ×$\frac{3}{4}$-in.-long stilbene) placed one on the transmission and one on the reflection side of the scatterer at distances varying from 6 to 10 in. The crystals were oriented as shown in Fig. 1. The scatterer to crystal distance varied with detection angle and was set at the maximum consistent with a neutron background/effect ratio less than two. We used pulse-shape discrimination to suppress gamma-ray background and integral discrimination to bias out inelastically scattered neutrons. Worst conditions occurred at the lowest neutron energy used (≈0.5 MeV). The resulting neutron pulse spectra are given in Fig. 2.

To facilitate background subtraction, the scatterers were suspended by thin wires from an overhead crane so that they could be moved in and out of the beam at each neutron energy (see Fig. 1).

Total Cross-Section Measurements

The same neutron beam, source shielding, collimation, and gamma suppression described above were used in measuring total cross sections.

Neutrons were detected in this case by a stilbene crystal with dimensions $\frac{1}{2}$-in. diam × $\frac{1}{2}$ in. long, mounted to measure transmission of the direct beam. Each scatterer was a right parallelepiped whose area normal to be beam (≈1 sq. in.) was sufficient to shield the crystal from direct neutrons. (Neutrons were produced over a proton beam spot area of about $\frac{1}{4}$ in. × $\frac{1}{4}$ in.) The samples were 10 in. from the collimation (28 in. from the neutron source) and 20 in. from the crystal. Sample thicknesses were chosen to allow approximately 60% neutron transmission at energies of interest in the experiment.[24] The sample and a 9-in.-long, 1-in.-diam tungsten shield were mounted on thin supporting rods above the ends of two arms of a rotatable horizontal cross. A third arm had only a dummy supporting rod attached. It was possible to count transmitted, background, and direct neutrons in sequence at each neutron energy by rotating the cross.

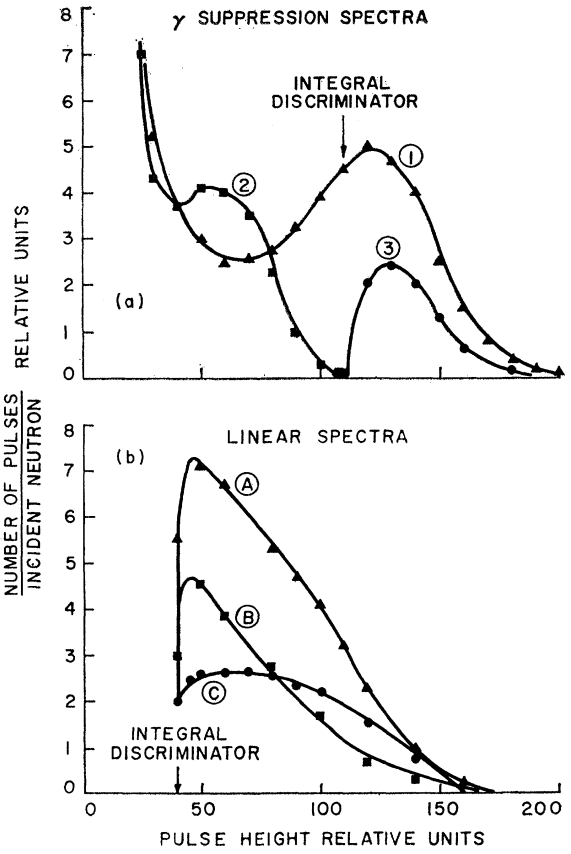

FIG. 2. Pulse spectra at neutron energy of 0.5 MeV. (a) Output of the gamma-suppression circuit: (1) With the crystal in the neutron beam. (2) With the proton beam blocked from hitting the tritium target, and a Na^{22} gamma source near the crystal. (3) With the crystal in the neutron beam and a Na^{22} gamma source near the crystal, and with the pulse-height analyzer gated by a coincidence between pulses from integral discriminators in both linear and gamma-suppression channels. (b) Linear output: The following spectra were taken with the crystal in a typical experimental position and with the pulse-height analyzer gated as in spectrum (a) (3). A. With the Li scatterer in the beam. B. With the scatterer in the "Out" position. C. Spectrum of elastically scattered neutrons, A–B.

DATA REDUCTION AND ANALYSIS

Data Averaging

The original data for differential-scattering experiments on zirconium, cerium, and barium showed

[24] H. H. Barschall, Rev. Mod. Phys. 24, 120 (1952).

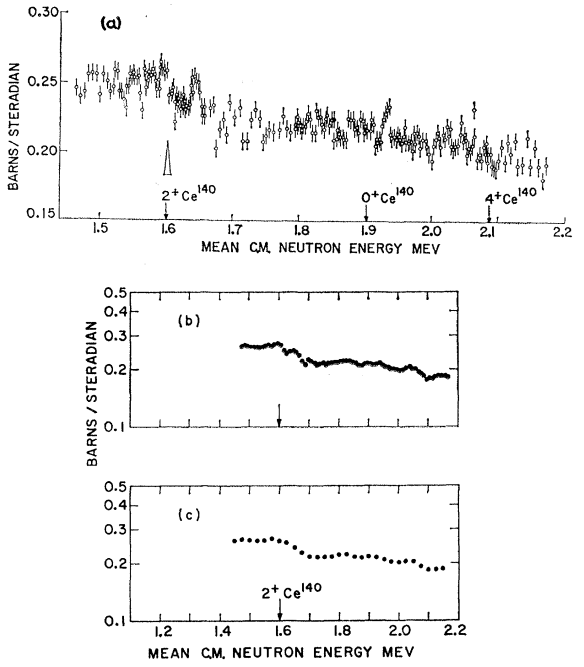

FIG. 3. Neutron differential elastic (90°) cross section of natural cerium for three widths of energy-averaging interval. (a) Original data; $\Delta E=7$ keV; statistical errors $\pm 7\%$. (b) Same data averaged over $\Delta E=25$ keV; statistical errors $\pm 2.5\%$. (c) Result of a larger averaging interval, $\Delta E=50$ keV; statistical errors approximately $\pm 1\%$. The averaging in (c) was selected as the standard for cusp analysis of cerium. The loss of structural detail upon successive averaging is apparent.

reproducible fluctuations, in addition to a well-defined drop in magnitude over a broad region above reaction thresholds. Energy averaging the original data did not mask the essential structure or features. Figure 3, where differential elastic cross-section data from a cerium experiment have been used, illustrates this point. Therefore, we were able to improve the statistical accuracy, without significant loss of structural detail, by using a thicker tritium target and also to establish a standard energy-averaging interval ($\Delta E=50$ keV) for presenting measurements at many angles.

In the experiments with lithium and iron, where we hoped to observe pure Wigner-cusp effects, we could not use data averaging procedures. The magnitude of resonance-like structure in the cross sections exceeded that expected of cusp effects; in the experiments on iron, the structure was particularly marked. A successful search for a cusp effect would depend upon distinguishing this structure from a true cusp effect. Hence, optimum energy resolution was essential in this case. Fig. 4, which gives iron total cross-section measurements, shows that use of 25-keV incident-neutron-energy resolution washed out significant structure observed in experiments with 7 keV spread in incident-neutron energy.

In addition to washing out structure, a poor-resolution incident beam also has the well-known effect of distorting sharp features in cross sections. Figure 4 shows a feature shift of about +10 keV as the result of using 25-keV compared to 7-keV energy resolution. This amount of shift would make a cusp analysis impossible.

In reporting some of the lithium differential cross sections we have energy averaged the data for clarity in presentation. It is clear from the foregoing discussion that in so doing we conceded that there was no noticeable cusp effect in the data and that remaining structure must be attributed strictly to the elastic scattering cross section of the lithium nucleus.

Data Analysis

Differential Cross Sections

The basic data consisted of counts $C=C_I$ (scatterer-in)$-C_0$ (scatterer-out), the detection efficiency measured in the calibration run, and geometrical factors. The energy loss in the lab system of elastically scattered neutrons required an angle-dependent correction to the response measured with the crystal in the direct beam. Expressed in mean center-of-mass (c.m.) coordinates and energies, the measured differential elastic scattering cross section is

$$d\sigma_{\text{c.m.}}[\bar{\theta}(\text{c.m.}),\bar{E}(\text{c.m.})]/d\Omega = (R_x^2/A_s)\epsilon_2(R_x)\epsilon_3\epsilon_4(\bar{E},\bar{\theta})[f_D(\bar{E})/f_D(\bar{E}-\bar{E}_R)] \sigma_T[1-\exp(-n\sigma_T d)]^{-1}KC(\bar{E})/C_c(\bar{E}), \quad (22)$$

where R_x is the crystal to scatterer distance, A_s is the scatterer area projected prependicularly to the beam axis, $\epsilon_2(R_x)$ is a correction for the deviation from inverse-square-distance behavior of the crystal response to neutron flux, ϵ_3 symbolizes the conversion from laboratory to center-of-mass coordinates, $\epsilon_4(\bar{E},\bar{\theta})$ is a correction for the difference between intrinsic crystal efficiency at the lab energies of direct and of elastically scattered

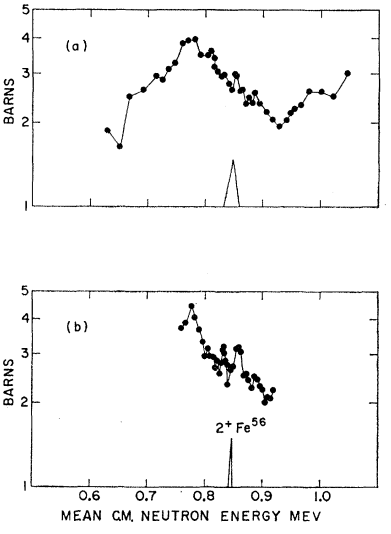

FIG. 4. The total neutron cross section of natural iron, using neutron beams of two energy spreads: (a) $\Delta E=25$ keV; (b) $\Delta E=7$ keV. The size of the symbol indicates the size of the statistical errors. The solid line connecting the points has been drawn for easier recognition of the results and is not meant to represent the true fluctuations.

neutrons, $[f_D(\bar{E})/f_D(\bar{E}-\bar{E}_R)]$ is a correction due to the fixed integral discriminator bias on linear-neutron pulses, reflecting the degree to which the counted fraction of the total linear pulse spectrum is different for direct and for elastically scattered neutrons, $\bar{E}_R$ is the recoil energy of the residual nucleus, σ_T is the total cross section of the scatterer material, nd is the number of scattering nuclei per unit area, $C(\bar{E})$ are the effect counts, $C_c(\bar{E})$ are the calibration counts, taken with the scintillation crystal in the beam, and K is a constant normalizing the effect and calibration counts to the same accumulated proton charge. In order to make a detailed comparison of gross structure, cusp effects in cross sections, or angular distributions with theory or with other experimental work, corrections for multiple scattering and finite scatterer effects were applied. A detailed discussion of the data analysis and corrections is given in Ref. 25.

Total Cross Sections

The data analysis for total cross sections is described by

$$\sigma_T[\bar{E}(\text{c.m.})]=(nd)^{-1}\epsilon_3 \ln[(C_D-C_B)/(C_T-C_B)], \quad (23)$$

where $\sigma_T[\bar{E}(\text{c.m.})]$ is the total cross section as a function of mean center-of-mass neutron energy, ϵ_3 is (as before) a symbol of the conversion of the energy dependence from lab to c.m. frame, nd is the number of nuclei per unit area in the sample, ln means natural logarithm, C_D is the number of direct neutron counts, C_B is the number of background counts, C_T is the number of transmission counts, and where C_D, C_B, and C_T are all functions of neutron energy and are all normalized to a fixed accumulated proton charge.

Error Analysis

Contributions to the uncertainty in the absolute magnitude of the differential elastic cross sections were present in each factor of Eq. (22).

Statistical errors entered the results through the factor C/C_c. Those in C_c were negligible. Errors in C are separately decreased in the figure captions for each set of experimental data. In general, the statistical errors were rather small (from 1 to 3%); hence, they had little effect on the precision of the absolute differential cross-section measurements.

We concluded that, exclusive of statistical errors and those errors associated with multiple scattering corrections, the absolute differential cross sections of zirconium, barium, and cerium were known to within ±14%, of iron to within ±16%, and of lithium to within ±19%.

Exclusive of statistical errors, which are given separately for each experiment, the uncertainty in our absolute total cross-section measurements was ±4%.

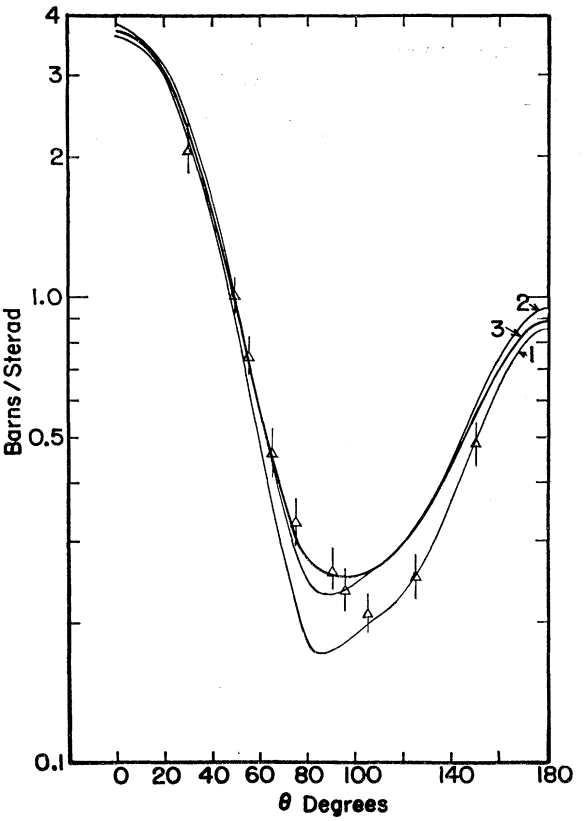

FIG. 5. Angular distribution of neutrons elastically scattered from natural cerium at $\bar{E}(\text{c.m.})=1.6$ MeV. Curve 1: An optical-model prediction by Moldauer (see Ref. 18). Curve 2: Curve 1 modified with a multiple scattering correction. Curve 3: Curve 2 modified with calculated experimental finite-scatterer effects. Triangles are experimental points from the present experiment. Note that the ordinate does not represent true differential cross sections, because multiple scattering and finite scatterer corrections have not been applied to the experimental cross sections, but to the theoretical cross sections.

EXPERIMENTAL RESULTS AND COMPARISON WITH THEORY

Energy and Angle Dependence of the Cross Sections

Although the basic purpose of the experiment was to search for threshold effects in neutron cross sections, data such as angular distributions and differential elastic and total cross sections were obtained, which are interesting in their own right, exclusive of possible cusp effects.

The measured angular distribution of 1.6-MeV neutrons scattered elastically from natural cerium is presented in Fig. 5. The data points are cross plotted from measurements as a function of energy at separate angles. As shown in the figure, an optical-model prediction of Moldauer,[18] modified for multiple-scatter-

[25] J. T. Wells, Ph.D. thesis, Stanford University, 1963 (University Microfilms, Inc., Ann Arbor, Michigan). (In all Wigner cusp expressions in this reference the quantity $\mathfrak{F}$, used in the present paper, has been taken to be unity.)

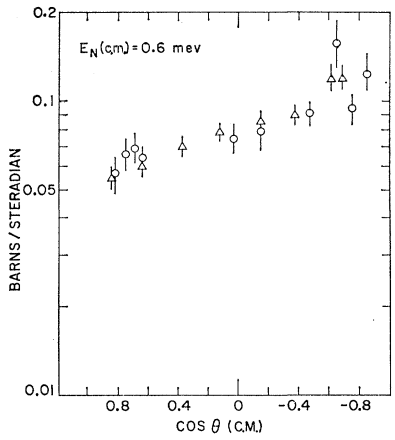

FIG. 6. Angular distributions of neutrons elastically scattered from natural lithium at $\bar{E}$(c.m.) =0.6 MeV. Open circles are data from the present experiment. The data are not corrected for multiple scattering. Triangles are data from Ref. 28.

ing and finite-scatterer effects agrees very well in shape and, except at back angles, in magnitude, with these data.

Figure 6 shows the measured angular distribution of 600 keV (c.m.) neutrons elastically scattered from natural lithium. The shape of the distribution is interesting, being peaked backwards, presumably as a result of interference between the strong p-wave resonance[26] at 0.25 MeV and an s-wave background. This backward peaking means that one should look at forward angles for cusp effects, because the theoretical (above threshold) percentage effect is inversely proportional to $(d\sigma/d\Omega)^{1/2}$ [see Eq. (12)].

In Fig. 7 we show some of the differential cross section data, versus energy, from which the angular distribution, Fig. 6, was cross plotted. At the lower energies the upper edge of the p-wave resonance[26] at 0.25 MeV is in evidence. The wavy structure in all the cross sections is probably not an experimental effect; it is quite surprising, because for a light nucleus such as lithium one might expect rather smoothly varying cross sections at these energies, except for isolated resonances. The inelastic cross section to the first excited state of Li^7, as measured by Freeman, Lane, and Rose[27] shows similar structure.

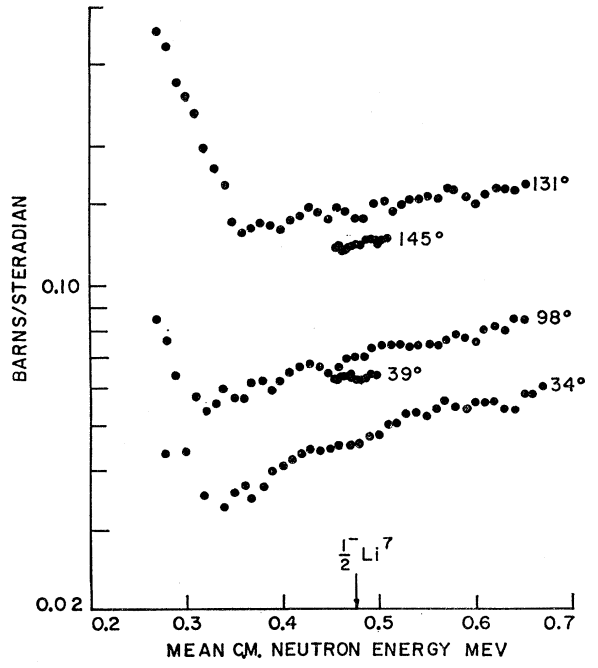

FIG. 7. Neutron differential elastic cross sections of natural lithium versus energy for five angles, in center-of-mass coordinates. The data are not corrected for multiple scattering. The original experimental results have been energy averaged. (Averaging interval ≈10 keV for the 39° and 145° data, and ≈20 keV for the other angles. The statistical errors in these points are approximately 1%.

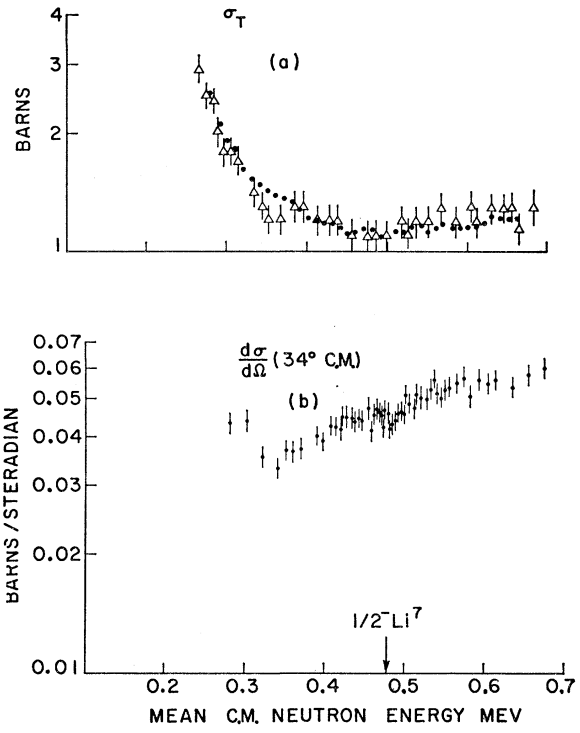

FIG. 8. Neutron cross sections of natural lithium versus energy. (a) Total neutron cross section; triangles are data from Ref. 28 and solid circles are the energy-averaged (ΔE=20 keV) data from the present experiment. (b) 34° (c.m.) differential elastic cross section of the present experiment.

Energy and Angle Dependence of Threshold Features

We discuss here the experimental results as they pertain to Wigner and "energy-averaged" Wigner cusps.

Lithium (92.6% Li^7)

The largest percentage cusp effect in $d\sigma/d\Omega$ is expected at forward angles, where $d\sigma/d\Omega$ is smallest. Figure 8(b)

[26] *Energy Levels of Nuclei*, edited by K. H. Hellwege (Springer-Verlag, Berlin, 1961), Vol. 1, Group I.

[27] J. M. Freeman, A. M. Lane, and B. Rose, Phil. Mag. 46, 17 (1955).

shows that some structure is indeed present at 34° (c.m.) in the vicinity of 0.478 MeV, the energy of the first excited state of Li^7. However, using the reaction cross section magnitude of Freeman, Lane, and Rose,[27] and the applicable theory [Eqs. (6) to (9)], we find that the observed effect was at least a factor 5 too large to be explained as a Wigner cusp; $\Delta d\sigma/d\Omega$ is calculated to be approximately 2% 50 keV from threshold. Figure 8(a) compares our measurement of lithium total cross section with that from Howerton's compilation.[28] Although the two sets of data agree, no Wigner cusp is evident in either. We had hoped to see an effect in the total cross section, because the results of Lane *et al.*[29]

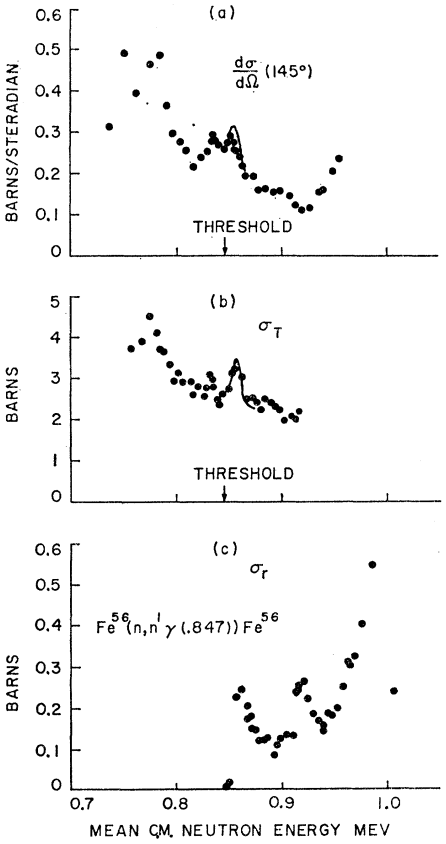

FIG. 9. (a) Neutron differential elastic (145°) cross section of natural iron versus energy. (b) Total neutron cross section of natural iron. (c) Reaction cross section Fe^{56} [n, $n'\gamma$ (0.847 MeV)] Fe^{56}. Statistical errors are the size of the symbols. The smooth curves show "differential scattering cross section without threshold effect," which results by removing a calculated Wigner cusp effect under one possible assumption for the phase of the scattering amplitude. *Note added in proof.* The cross sections indicated in part (c) should be increased by 20%.

appear to show a break near 0.5 MeV (lab energy) in the coefficient B_0 of the Li^7 cross-section expansion.

[28] R. J. Howerton, University of California Report UCRL-5226, revised, 1959 (unpublished).

[29] R. O. Lane, A. S. Langsdorf, Jr., J. E. Monahan, and A. J. Elwyn, Ann. Phys. (N.Y.) 12, 128 (1961); also Argonne National Laboratory Report ANL-5567, revised, 1961 (unpublished).

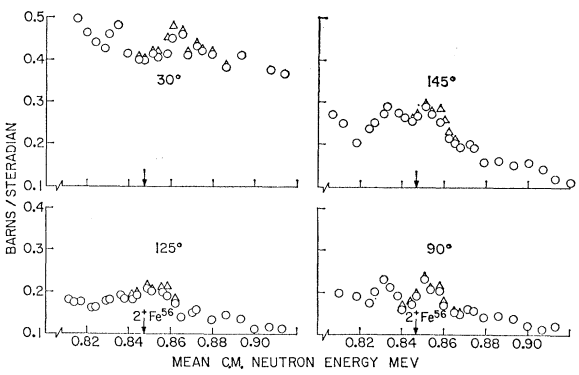

FIG. 10. Neutron differential elastic cross sections of natural iron versus energy for four angles. The data are not corrected for multiple scattering. Statistical errors are indicated by the symbol size. Open triangles show the result of removing a calculated Wigner cusp effect, under one possible assumption on the phase of the scattering amplitude.

But the energy-scale change in Fig. 2 of Ref. 29 at about 0.5 MeV may bias this interpretation of their data.

Iron (91.7% Fe^{56})

With iron distinct features appear in all cross sections at the energy of interest (2^+ first excited state Fe^{56}, 0.847 MeV). This is exemplified in Fig. 9 where a resonance feature appears, apparently at an identical energy (just above 0.847 MeV) in the total cross section, in the 145° differential elastic cross section and in the reaction cross section $Fe^{56}(n,n')Fe^{56*}$ (0.847 MeV). The latter cross section was measured by Tucker, *et al.*, using the same tritium target.[20] Another resonance feature just below threshold is evident in these data, and in all the differential cross sections at other angles investigated (see Fig. 10). That this below-threshold feature could not be interpreted as a Wigner-cusp effect was a disappointment to us.

Application of the most general theory is hopeless because of the large number of unknown phases. At least six phases can contribute to the cusp expression, even with a restriction on participating incident partial waves to those with orbital angular momentum l less

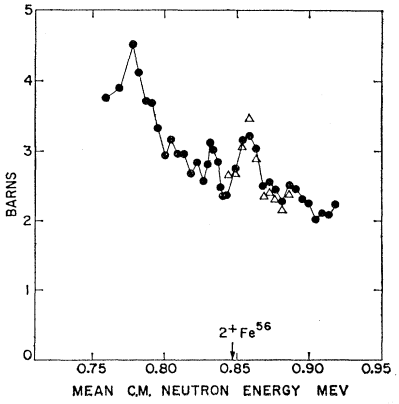

FIG. 11. Total cross section of natural iron. The size of the statistical errors is indicated by the size of the symbol. Triangles show the result of removing a calculated Wigner-cusp effect under one possible assumption on the phase of the scattering amplitude.

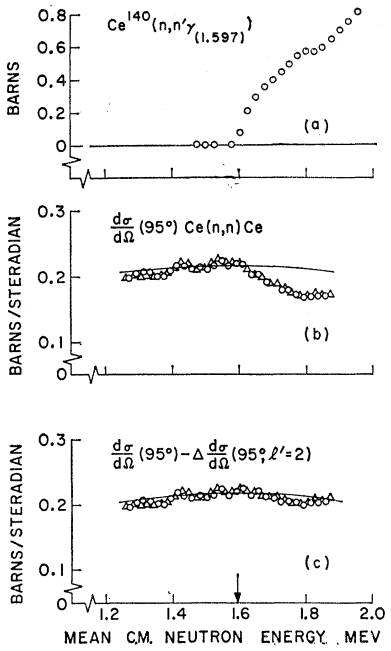

FIG. 12. The experimental data for the analysis of an "energy-averaged" Wigner cusp in cerium. (a) Energy-averaged ($\Delta E=40$ keV) experimental inelastic cross section $Ce^{140}[n, n'\gamma(1.597\text{ MeV})]Ce^{140}$ from Ref. 20. (b) Original data for elastic 95° scattering of neutrons from natural cerium. The two symbols demonstrate the reproducibility of the data on successive interleaving energy runs. The size of the symbols indicates the statistical errors. (c) Same data as (b) corrected, point by point, for a calculated "energy-averaged" Wigner cusp. The smooth curves in (b) and (c) are optical-model predictions of Campbell *et al.* (see Ref. 30), normalized at 1.6 MeV.

than 3. A reasonable and tractable special case of the theory was used; namely, the elastic scattering and reaction were both assumed to be dominated by a single (isolated) resonance. This special assumption allowed cusp analysis only over a narrow energy region, entirely above threshold. The resulting calculated cusp effect was subtracted from the differential elastic and total cross sections, leaving the "cross sections without reaction effect," $d\sigma^0/d\Omega$ and $\sigma_T{}^0$, respectively [see Eqs. (6) and (10)]. The results of this analysis are superimposed on the data in Fig. 10 for differential cross sections and in Fig. 11 for the total cross section. The results are neither startling nor conclusive, although by removal of the cusp effect the peak energies and widths of the above threshold resonance in the differential elastic, total and inelastic cross sections can be brought into exact coincidence.

Cerium-Barium-Zirconium

We consider now the results obtained for targets of higher atomic number in the region where statistical models are expected to apply because compound resonances are closely spaced. The theory of "energy-averaged" Wigner cusps is then expected to apply.

Composite data for cerium, given in Fig. 12, is representative of the cusp analyses we present for all three elements. A special feature of this figure, however, is that we present the original data, to show the degree of scatter on interleaving runs. This and other figures in this group also show cross section trends predicted by the optical model. These were obtained from the work of Campbell *et al.*[30] The optical-model shapes were interpolated from very few points given in the reference and should not be considered a precise computation. They were normalized to the experimental data at threshold energy. The magnitudes of the predicted cross sections[30] were consistent within the estimated experimental errors.

A cusp effect is quite apparent in Fig. 12(b) by comparison of the optical model trends with the experimental cross section. To compare the magnitude of the cusp effect with theory, one could subtract the experimental cross section from the optical-model prediction and plot the difference as a function of neutron energy. But, as mentioned before, the optical-model trends are somewhat uncertain and, furthermore, the experimental cross section has natural fluctuations, which will be discussed below. Hence, it was thought more appropriate to remove from the experimental cross sections the theoretical cusp effect and to show (a) that in the resultant curve there would be no more cusp effect, at least within the natural fluctuations of the cross section; and (b) that the resultant curve would follow the optical-model trend which theoretically represents the cross section without threshold effects.

The procedure for removing a theoretical cusp from the measured cross section was to multiply the reaction cross section (i.e., inelastic neutron scattering cross section) by the isotopic percentage of the isotope of interest, by the appropriate multiple scattering and finite scatterer correction and by the theoretical angle dependent factor. This negative quantity was subtracted from the experimental data [see Eq. (6)].

Cerium (88.5% Ce^{140})

In the case of cerium, Eq. (21) applies. Tucker, *et al.*, measured the reaction cross section [Fig. 12(a)] $Ce^{140}(n,n')Ce^{140*}$ (1.60 MeV).[20] As previously mentioned, incident d waves dominate the reaction to at least 150 keV above threshold, hence $l'=2$ as in Eq. (21). The results of removing the theoretical cusp effect are shown in Fig. 12(c). There is little doubt that the theoretical "energy-averaged" Wigner-cusp expression, with $l'=2$ and R_J' as chosen for Eq. (21) is a satisfactory description of the change at threshold.

Equations (18), and (6) to (8) predict that if incident s waves were imagined to dominate this reaction, rather than the actual d waves, the resulting expected cusp, at polar angle 90°, for example, would be a factor

[30] E. J. Campbell, H. Feshbach, C. E. Porter, and V. F. Weisskopf, MIT Lab. Nucl. Sci. Tech. Rept. No. 73, 1960 (unpublished).

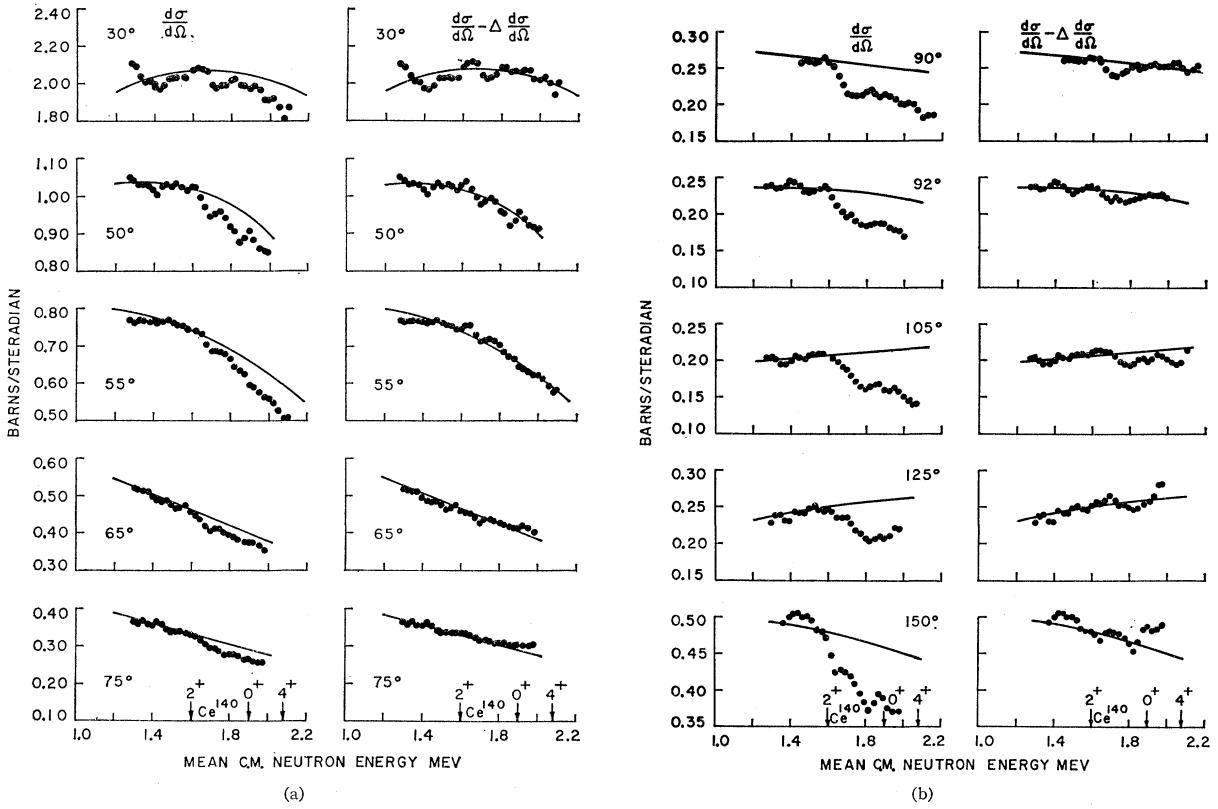

FIG. 13. (a) (b) The neutron differential elastic cross section of natural cerium versus energy for ten angles. The data are not corrected for multiple scattering. Statistical errors are ±1%. The points are an energy average ($\Delta E = 50$ keV) of the original experimental data. For each angle the left side is the measured cross section. The right side is the cross section with a calculated "energy-averaged" Wigner cusp removed. The calculation is based on the excitation of the 1.6-MeV state in Ce^{140}. No cusp contributions from the 0^+ (1.90-MeV) or 4^+ (2.08-MeV) states are included but these are expected to be small. The smooth curves are optical model predictions of Campbell, *et al.* (see Ref. 30) normalized at 1.6 MeV.

20/13 or about 50% larger. The plot corresponding to Fig. 12 (c), corrected for an expected $l'=0$ cusp, would show an upward break at threshold and would follow neither the below-threshold data trend nor the optical-model trend. Thus, we can conclude the reaction is not dominated by incident s waves. This type of analysis can be useful in assigning excited state spins.

The differential elastic cross section of cerium was measured at ten angles, versus energy. These results are shown in Fig. 13. The points obtained after removing a calculated cusp are also given for each angle. In all cases, the adjusted data so obtained follow the trend of the below-threshold data and the fluctuations in these are the same above and below threshold. In general, the modified cross sections agree nicely with the optical-model curves; that is, they follow what the theory defines as "cross section without reaction." There is no reason to expect this agreement to be perfect, since the optical model was constructed to explain gross structures only, over a wide range of atomic number and energy.

We should recall the assumption, made for Eq. (21), that the fraction (called R_J') of the reaction probability for proceeding from compound nucleus states of a particular J' is the same as the fraction of the dominant-incident partial-wave states which have $J=J'$. Other assumptions for R_J' lead to cusp-magnitude predictions differing from those used here by as much as 30%, at certain angles. It is possible that an experiment more refined than the present one could be used to measure R_J'. Such a measurement could assist in the understanding of neutron-nucleus interaction mechanisms, particularly if it turned out that a particular reaction preferred one value of compound nucleus J' to another, even though resonances were closely spaced and possibly overlapping. Such a refinement would depend critically upon the precision to which the absolute cross sections are known.

Barium (71.7% Ba^{138})

The measured cross sections of barium and the results of the appropriate cusp analysis are compiled in Fig. 14. The reaction cross section $Ba^{138}(n,n')Ba^{138*}$ (1.427 MeV) was measured by Tucker *et al.*[20] Again the spin of the first excited level is 2^+ and the ground state 0^+. That s-wave neutrons dominate the reaction over the energy region of interest is not so clear in this case,

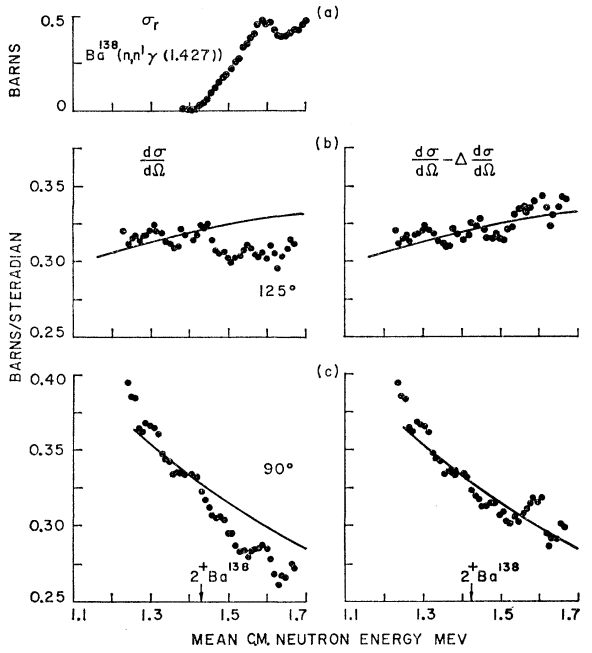

FIG. 14. Neutron scattering cross sections and cusp analysis for barium. (a) Energy-averaged ($\Delta E=20$ keV) inelastic cross section for Ba^{138} [n, $n'\gamma$(1.427 MeV)] Ba^{138}, obtained from Ref. 20; statistical errors are $\pm 5\%$. The left side of (b) and (c) are an energy average ($\Delta E=25$ keV) of the original experimental data for natural barium. The data are not corrected for multiple scattering. Statistical errors are $\pm 1\%$. The right sides of (b) and (c) show the results of removing calculated "energy-averaged" Wigner cusps. The smooth curves are optical-model predictions of Campbell *et al.*, normalized at 1.427 MeV (see Ref. 30).

since the reaction shape is distorted by resonance-like structure. However, optical-model calculations show that barium is near a maximum in the s-wave strength function.[19] As in cerium then, the reaction is considered to proceed by the $l'=2$ incident partial wave. The results of theoretical comparison are satisfactory. The cusp effect is smaller than in cerium because of the smaller isotopic percentage and the smaller reaction cross section near threshold. From Fig. 14(b) we see that it would be difficult to distinguish a cusp at all were it not for a comparison with the optical-model trend which happens to be rising.

Zirconium (51.5% Zr^{90})

The measured cross sections of zirconium and the results of cusp analysis are compiled in Fig. 15. The inelastic reaction $Zr^{90}(n,n')Zr^{90*}$ (1.75 MeV) was measured by Tucker *et al.*[20] The spin of the 1.75-MeV first excited state is 0^+ and the ground state 0^+. Moldauer[18] showed that p-wave outgoing neutrons dominate the reaction not far above threshold. Hence, we assume that the reaction proceeds from incident p waves, i.e., $l'=1$. For Zr^{90} the low isotopic percentage and small reaction cross section near threshold combine to produce a small calculated cusp effect. At 60° polar angle the predicted cusp effect is too small to be distinguished in the data. Note also that at 60° the optical-model trend does not agree well with the measured cross section slope. At 130° the cusp is barely distinguishable, but the theoretical cusp fit appears to be satisfactory.

Total Cross Sections

The theoretical "energy-averaged" Wigner cusps which were used to explain the preceding experimental results (Ce, Ba, Zr) are based on the same assumptions that underlie the optical model. These assumptions also lead to predictions that the energy average of the *total* cross sections should be smooth across thresholds [see Eq. (19)]. Our measurements of the total cross sections of cerium and barium are given in Fig. 16. The predicted cusp effect for the total cross section of zirconium—even if the energy-averaged theory would not apply—would be so small that we did not investigate this case. For completeness, though, the zirconium total cross-section data from Howerton[28] is presented in Fig. 16, showing the inadequacy of widely spaced energy points for the present study. The data for barium and cerium, taken with an energy spread of about 30 keV, are certainly not smooth functions of energy. Yet the mean values of

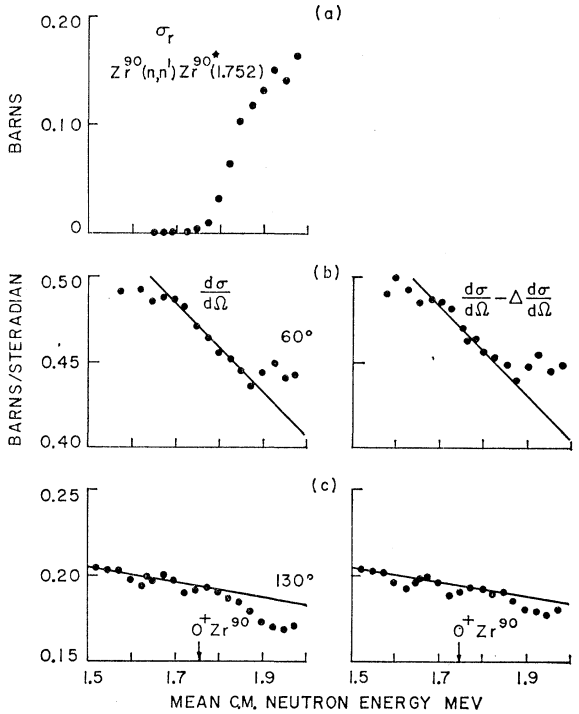

FIG. 15. Neutron cross sections and cusp analysis for zirconium. (a) is a 40-keV average of the reaction cross section $Zr^{90}(n,n')Zr^{90*}$ (1.75 MeV), obtained from Ref. 20. Statistical errors are $\pm 5\%$. The left sides of (b) and (c) are an energy average ($\Delta E=50$ keV) of the measured cross sections for natural zirconium. The data are not corrected for multiple scattering. Statistical errors are $\pm 1\%$. The right sides of (b) and (c) show the results of removing calculated "energy-averaged" Wigner cusps. The smooth curves are optical model predictions of Campbell *et al.*, normalized at 1.75 MeV (see Ref. 30).

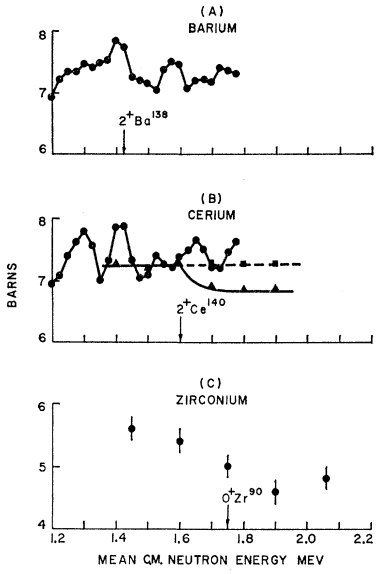

FIG. 16. Neutron total cross sections for natural barium, (A); cerium, (B); and zirconium, (C). Statistical errors are indicated by the size of the symbols. The data on barium and cerium were measured in the present experiment. The data on zirconium is taken from Ref. 28. In (B) the circles are the measured total cross section of cerium; the triangles are integrated elastic cross sections, corrected for multiple scattering; and the squares are the sum of the integrated elastic and of the reaction cross section (corrected for isotopic percentage) $Ce^{140}[n, n'\gamma(1.6\ \text{MeV})]Ce^{140}$ from Ref. 20.

these cross sections do not seem to drop markedly as threshold is crossed, suggesting agreement with the theory. If the theory of "energy-averaged" cusps did not apply, but one assumed instead a pure Wigner-cusp phenomenon, the cusp predicted is at most a 5% effect which would be masked by the fluctuations. Hence, the total cross section data cannot be considered a verification of either assumption.

That the fluctuations are not experimental is supported by the differential cross-section data for cerium at forward angles (Fig. 13) which show the same structure. Note that the structure does not contain recognizable resonance shapes. It is possible that the considerations of Ericson on statistical fluctuations in cross sections might apply here.[31] He shows that if a compound system is characterized by many overlapping resonances, each of width Γ, and with random phase of the value quantities γ_λ of resonance theory,[21] cross sections would have a fluctuating structure of average width Γ.

In the case of cerium only, sufficient differential elastic data were taken to permit integration over all solid angles. The total elastic cross sections so obtained for several energies, after correction for multiple scattering, are plotted in Fig. 16 (B). The drop at threshold (1.6 MeV), produced by the drop in all the differential cross sections, is evident. In any theory of threshold effects, flux conservation alone requires the total elastic cross section to drop above threshold for a reaction. It is reassuring that, when the inelastic scattering cross section is corrected for isotopic percentage and added to the integrated elastic cross section, the resultant cross section (i.e., the total cross section) is smooth across threshold. The agreement in magnitude between the latter curve and the directly measured total cross section is considered somewhat fortuitous.

[31] T. Ericson, Phys. Rev. Letters **5**, 430 (1960). Also T. Ericson, unpublished lectures, Varenna, Italy, 1961; and International Conference on Direct Interaction and Nuclear Reaction Mechanisms, Padna, 1962 (unpublished).

CONCLUSIONS

The experiments have shown that under suitable conditions the threshold effects expected in neutron elastic scattering can be observed. From an experimental point of view, particular attention must be paid to the choice of energy resolution consistent with observing a cusp effect in reasonable time.

Explicit theoretical expressions have been obtained for expected Wigner and "energy-averaged" Wigner-cusp effects in differential elastic and total cross sections under general angular-momentum conditions, within some simplifying restrictions imposed in the derivation. The effects were found to be contained in the coefficients, B_L, of the Blatt-Biedenharn formulation of the general scattering problem.[12] Since many survey experiments involving neutron scattering have been analyzed in terms of the B_L coefficients, we make the obvious suggestion that such results be examined near excited-state energies for possible tests of cusp theory.

The Wigner cusp in lithium cross sections was expected to be an approximately 2% effect, 50 keV from threshold. Our experiment was not sufficiently refined to pick out an effect of this size.

Resonance structure in the measured cross sections of iron made a Wigner-cusp interpretation ambiguous. Features occurred at the threshold energy, but their analysis in terms of cusp theory was inconclusive.

The measured differential elastic cross sections of Zr, Ba, and Ce dropped at inelastic thresholds. Analysis of the drops in terms of "energy-averaged" Wigner-cusp theory resulted in good agreement with experiment. This indicates that the usual energy-averaging assumptions underlying the theory are indeed applicable to these nuclei. Also, the cusp theory[7] shows that there cannot be a large amount of direct interaction between incident neutrons and these nuclei at the neutron energies used in these experiments ($\leqq 2$ MeV), or else below-threshold effects would also be seen.

ACKNOWLEDGMENTS

The authors are indebted to Dr. P. A. Moldauer and Professor J. D. Walecka for enlightening discussions on the interpretation of experimental cusps. Miss B. Luppino contributed substantially in the reduction and analysis of the data. We express our appreciation to

K. E. Williams and R. Brown for their assistance in preparing some necessary electronic equipment.

APPENDIX A

We wish to derive expressions for Wigner cusps in differential elastic and total cross sections, under the assumptions made in the main text.

Wigner Cusps in Differential Elastic Cross Sections

The partial reaction cross section given as Eq. (5) is essentially the statement that the S matrix is unitary. By inverting Eq. (5), the S-matrix element of the dominant incident partial wave may be written as

$$S_{l's';l's'}{}^{J'}=(\exp 2i\delta_{l's'}{}^{J'})(1-\sigma_{rl's'}{}^{J'})^{1/2} \approx(\exp 2i\delta_{l's'}{}^{J'})(1-\sigma_{rl's'}{}^{J'}/2), \quad \text{(A1)}$$

if $\sigma_{rl's'}{}^{J'}\ll 1$.

Equation (A1) defines $2\delta_{l's'}{}^{J'}$ as the (real) phase of the S-matrix element $S_{l's';l's'}{}^{J'}$ above threshold for the reaction. To simplify the notation, we have expressed $\sigma_{rl's'}{}^{J'}$ in units of $\pi\lambda\!\!\!^{-}{}^2 g_{s'}{}^{J'}$. This normalization will be used only in this Appendix.

Equation (A1) is certainly valid above threshold. The usual procedure[2,3] is to expand the complete phase (which may have real and imaginary parts) of $S_{l's';l's'}{}^{J'}$ in energy about threshold. One consequence of this procedure is that the fixed value of the real phase at threshold appears in the final expressions. On the other hand, Eq. (A1) is quite general and there is no reason to assume that the form of Eq. (A1) should not persist even away from threshold (above threshold). Consequently, we shall allow the real part of the phase of **S**, i.e. 2δ, as well as σ_r, to vary over the energy region of interest, if the physical situation requires that they do so. This leaves us free later to examine the consequences of energy averaging over a cusp region where the phase 2δ and the cross section σ_r might be fluctuating rapidly because of the presence of many narrow resonances.

Using R-matrix theory, it can be shown that the S matrix can always be written in a form equivalent to Eq. (A1) if $l_0=0$, regardless of whether the energy is above or below threshold.[7] An analytic continuation in energy across threshold always exists, even in the presence of many narrow and possibly overlapping resonances which would produce rapid variation with energy in the phase and in the reaction cross section.

The notation used in Ref. 7 is somewhat misleading, though. Although above threshold the symbol $\sigma_{rl's'}{}^{J'}$ indeed represents the experimentally measured reaction cross section, the functional form of the equivalent expression below threshold must be determined theoretically. This is best seen by referring to Eqs. (21a) or (25) in Ref. 7, which for $l_0=0$ can be seen to require

$$\sigma_r=k_0F(E_\alpha), \quad E_\alpha>E_T, \quad \text{(A2)}$$

where $k_0=(E_\alpha-E_T)^{1/2}$ [in units of $(2M/\hbar^2)^{1/2}$]; E_α is the c.m. energy of the incident neutron and E_T the reaction threshold. $F(E_\alpha)$ is a function of the R matrix, which depends only on E_α. In the simplest situation $F(E_\alpha)$ has the shape of a Breit-Wigner resonance. It turns out[7] that the below-threshold expression can be obtained by the substitution $k_0\to i|k_0|$ and, hence, the appropriate expression corresponding to Eq. (A2) is

$$\sigma_r=i|k_0|F(E_\alpha), \quad E_\alpha<E_T. \quad \text{(A3)}$$

In order to identify the symbol σ_r with the experimental cross section, below and in the main text, we write

$$S_{l's',l's'}{}^{J'}\approx(\exp 2i\delta_{l's'}{}^{J'})\left(1-\tfrac{1}{2}\sigma_{rl's'}{}^{J'}\begin{Bmatrix}1\\ i\mathfrak{F}\end{Bmatrix}\right) \quad \text{(A4)}$$

where

$$\sigma_{rl's'}{}^{J'}=|k_0|F(E_T+|k_0|^2) \quad \text{(A5)}$$

and

$$\mathfrak{F}=F(E_T-|k_0|^2)/F(E_T+|k_0|^2). \quad \text{(A6)}$$

Following Newton,[2] the bracket $\begin{Bmatrix}A\\ B\end{Bmatrix}$ represents A if $E_\alpha>E_T$, and B if $E\alpha<E_T$.

In Ref. 7 it was shown that $\delta_{l's'}{}^{J'}$ depends only on E_α. Hence, it is reasonable to separate $S_{l's';l's'}{}^{J'}$ into two terms, i.e.,

$$S=S^0+\Delta S, \quad \text{(A7)}$$

where

$$S^0=\exp 2i\delta_{l's'}{}^{J'} \quad \text{(A8)}$$

can be interpreted as the "S-matrix element without reaction effects," if $l_0=0$.[7] When this term is substituted into Eqs. (1), (2), and (3), and the indicated sums are performed, the result is the "differential elastic cross section without reaction effects" which we designate by $d\sigma^0/d\Omega$. Also,

$$\Delta S=-(\exp 2i\delta_{l's'}{}^{J'})\tfrac{1}{2}\sigma_{rl's'}{}^{J'}\begin{Bmatrix}1\\ i\mathfrak{F}\end{Bmatrix} \quad \text{(A9)}$$

produces a cusp term. As the presence of the factor $\mathfrak{F}$ in the below-threshold part indicates, this breakup of the S-matrix element into two terms is not the result of a rigorous expansion about threshold energy in powers of k_0. It is rather an expansion in powers of $\sigma_r/(\pi\lambda\!\!\!^{-}{}^2 g)$ in the spirit of Eq. (A1), which allows the theory to predict approximate cusp effects, even where structure is present in the cross sections. By substituting S into Eq. (3) one obtains

$$\begin{aligned}\Delta B_L(s';s') &= (\tfrac{1}{4})\sum_{J_1}\sum_{l_1}\sum_{J'}Z^2(l_1J_1l'J',s'L)\,\mathrm{Re}\Big[(1-\exp 2i\delta_{l_1s'}{}^{J_1})^* \\ &\quad\times(\exp 2i\delta_{l's'}{}^{J'})\tfrac{1}{2}\sigma_{rl's'}{}^{J'}\begin{Bmatrix}1\\ i\mathfrak{F}\end{Bmatrix}\Big] \\ &\quad+\sum_{J'}\sum_{J_2}\sum_{l_2}Z^2(l'J'l_2J_2,s'L)\,\mathrm{Re}\Big[(\exp 2i\delta_{l's'}{}^{J'})^* \\ &\quad\times\tfrac{1}{2}\sigma_{rl's'}{}^{J'}\begin{Bmatrix}1\\ i\mathfrak{F}\end{Bmatrix}^*(1-\exp 2i\delta_{l_2s'}{}^{J_2})\Big],\end{aligned}$$

where $\sigma_{rl's'}{}^{J'}$ is still expressed in units of $\pi\lambda\!\!\!^{-2}g_{s'}{}^{J'}$ [see Eq. (A1)]. The sums over l_1, J_1, l_2, J_2 in Eq. (3) are reduced because of the assumption that a single incident wave l' is dominant in the reaction. Because

$$Z^2(l_1J_1l_2J_2,sL)=Z^2(l_2J_2l_1J_1,sL)$$

and $\mathrm{Re}(A^*B)=\mathrm{Re}(AB^*)$, we may combine these sums, changing dummy indices to obtain

$$\Delta B_L(s';s') = (\tfrac{1}{4})\sum_J\sum_l\sum_{J'} 2Z^2(lJl'J',s'L)\,\mathrm{Re}\Big[(1-\exp 2i\delta_{ls'}{}^J)^* \times(\exp 2i\delta_{l's'}{}^{J'})\tfrac{1}{2}\sigma_{rl's'}{}^{J'}\begin{Bmatrix}1\\ i\mathfrak{F}\end{Bmatrix}\Big]. \quad \text{(A10)}$$

Taking the real part in the last equation yields the desired result, Eq. (9) of the main text. In Eq. (9) units have been restored to $\sigma_{rl's'}{}^{J'}$. Substitution of Eq. (9) into Eq. (8) leads to the differential cross-section cusp term defined by Eqs. (6) and (7).

Wigner Cusps in Total Cross Sections

A Wigner cusp in the total cross section is defined by Eq. (10) to be

$$\sigma_T=\sigma_T{}^0+\Delta\sigma_T$$

where

$$\Delta\sigma_T=\int(\Delta d\sigma/d\Omega)d\Omega+\sigma_{rl'}\begin{Bmatrix}1\\ 0\end{Bmatrix}. \quad \text{(A11)}$$

Integration of $\Delta d\sigma/d\Omega$ [Eq. (7)] over all solid angles yields

$$\Delta\sigma_T=\sum_{s'=|I-i|}^{I+i}\frac{(2s'+1)}{(2I+1)(2i+1)}\frac{\lambda\!\!\!^{-2}}{(2s'+1)} \times 4\pi\Delta B_0(s';s')+\sigma_{rl'}\begin{Bmatrix}1\\ 0\end{Bmatrix}. \quad \text{(A12)}$$

Substituting

$$Z(lJl'J',s'0)=\delta_{ll'}{}^K\delta_{JJ'}{}^K(-1)^{J-s'}(2J+1)^{1/2},$$

where $\delta_{ll'}{}^K$ and $\delta_{JJ'}{}^K$ are Kronecker deltas, into the equation for ΔB_L (with $L=0$), Eq. (9), and putting this result into Eq. (A12), one obtains

$$\Delta\sigma_T=\sum_{s'=|I-i|}^{I+i}\frac{(2s'+1)}{(2I+1)(2i+1)} \times\sum_{J'=|l'-s'|}^{l'+s}\left(\frac{\pi\lambda\!\!\!^{-2}(2J'+1)}{(2s'+1)}\sigma_{rl's'}{}^{J'}\right) \times\begin{Bmatrix}-2\sin^2\delta_{l's'}{}^{J'}\\ -\mathfrak{F}\sin 2\delta_{l's'}{}^{J'}\end{Bmatrix}+\sigma_{rl'}{}^{J'}\begin{Bmatrix}1\\ 0\end{Bmatrix}, \quad \text{(A13)}$$

where we have explicitly indicated the units of $\sigma_{rl's'}{}^{J'}$ [see Eq. (A1)]. Finally, recognizing that the summations in Eqs. (A13) and (4) are identical, we may combine

$$\begin{Bmatrix}1\\ 0\end{Bmatrix}-\begin{Bmatrix}2\sin^2\delta_{l's'}{}^{J'}\\ \mathfrak{F}\sin 2\delta_{l's'}{}^{J'}\end{Bmatrix}=\begin{Bmatrix}\cos 2\delta_{l's'}{}^{J'}\\ -\mathfrak{F}\sin 2\delta_{l's'}{}^{J'}\end{Bmatrix}$$

and obtain the result, given in the main text as Eq. (11).

APPENDIX B

We wish to show that for the case of many resonances in the averaging interval one finds under certain conditions

$$\left\langle\sigma_{rl'}{}^{J'}2\sin\delta_l{}^J\begin{Bmatrix}\sin(2\delta_{l'}{}^{J'}-\delta_l{}^J)\\ \mathfrak{F}\cos(2\delta_{l'}{}^{J'}-\delta_l{}^J)\end{Bmatrix}\right\rangle \approx\begin{Bmatrix}\langle\sigma_{rl'}{}^{J'}\rangle\\ 0\end{Bmatrix}\delta_{ll'}{}^K\delta_{JJ'}{}^K, \quad \text{(17)}$$

where δ^K is the Kronecker delta. Expanding the left side of (17), we obtain

$$\left\langle\sigma_{rl'}{}^{J'}2\sin\delta_l{}^J\begin{Bmatrix}\sin(2\delta_{l'}{}^{J'}-\delta_l{}^J)\\ \mathfrak{F}\cos(2\delta_{l'}{}^{J'}-\delta_l{}^J)\end{Bmatrix}\right\rangle =\left\langle\sigma_{rl'}{}^{J'}\begin{Bmatrix}\sin 2\delta_{l'}{}^{J'}\sin 2\delta_l{}^J-\cos 2\delta_{l'}{}^{J'}2\sin^2\delta_l{}^J\\ \mathfrak{F}\cos 2\delta_{l'}{}^{J'}\sin 2\delta_l{}^J+\mathfrak{F}\sin 2\delta_{l'}{}^{J'}2\sin^2\delta_l{}^J\end{Bmatrix}\right\rangle. \quad \text{(B1)}$$

For simplicity, let

$$A=\sigma_{rl'}{}^{J'}\begin{Bmatrix}\sin 2\delta_{l'}{}^{J'}\\ \mathfrak{F}\cos 2\delta_{l'}{}^{J'}\end{Bmatrix},\quad B=\sigma_{rl'}{}^{J'}\begin{Bmatrix}-\cos 2\delta_{l'}{}^{J'}\\ \mathfrak{F}\sin 2\delta_{l'}{}^{J'}\end{Bmatrix},$$

$$a=\sin 2\delta_l{}^J,\quad \text{and}\quad b=2\sin^2\delta_l{}^J.$$

Then expression (B1) becomes

$$\text{(B1)}=\langle Aa+Bb\rangle. \quad \text{(B2)}$$

We now assume that the quantities A, B, a, and b may be written as the sum of a mean value and a fluctuating part; for example, $A=A^0+\Delta A$, where $\langle\Delta A\rangle=0$. Thus, expression (B2) may be written

$$\langle A^0a^0+B^0b^0+A^0\Delta a+a^0\Delta A+B^0\Delta b +b^0\Delta B+\Delta A\Delta a+\Delta B\Delta b\rangle. \quad \text{(B3)}$$

Meyerhof showed in Ref. 7 that under the random sign approximation

$$\left\langle\sigma_{rl'}{}^{J'}\begin{Bmatrix}-\cos 2\delta_{l'}{}^{J'}\\ \mathfrak{F}\sin 2\delta_{l'}{}^{J'}\end{Bmatrix}\right\rangle\equiv\langle B\rangle\approx 0. \quad \text{(16)}$$

Also,

$$\left\langle\sigma_{rl'}{}^{J'}\begin{Bmatrix}\sin 2\delta_{l'}{}^{J'}\\ \mathfrak{F}\cos 2\delta_{l'}{}^{J'}\end{Bmatrix}\right\rangle\equiv\langle A\rangle\approx 0$$

on the same basis as the proof of (16). Therefore, $A^0=B^0\approx 0$ and expression (B3) is reduced to

$$\langle \Delta A \Delta a + \Delta B \Delta b \rangle, \tag{B4}$$

where we have also used $\langle a^0 \Delta A \rangle = \langle b^0 \Delta B \rangle = 0$. ΔA and ΔB are functions of $\delta_{l'}{}^{J'}$ while Δa and Δb refer only to $\delta_l{}^J$. For $l \neq l'$ and/or $J \neq J'$, the fluctuation over the averaging interval in functions of $\delta_l{}^J$ are assumed uncorrelated to those in functions of $\delta_{l'}{}^{J'}$; thus, expression (B4) is equal to zero, and we have proved Eq. (17) for this case.

For $J=J'$ and $l=l'$ the left-hand side of Eq. (17) reduces to

$$\left\langle \sigma_{rl'}{}^{J'} \begin{Bmatrix} 2\sin^2\delta_{l'}{}^{J'} \\ \mathfrak{F}\sin 2\delta_{l'}{}^{J'} \end{Bmatrix} \right\rangle,$$

and we may use the result proved in Ref. 7,

$$\left\langle \sigma_{rl'}{}^{J'} \begin{Bmatrix} 2\sin^2\delta_{l'}{}^{J'} \\ \mathfrak{F}\sin 2\delta_{l'}{}^{J'} \end{Bmatrix} \right\rangle \approx \begin{Bmatrix} \langle \sigma_{rl'}{}^{J'} \rangle \\ 0 \end{Bmatrix} \tag{15}$$

which completes the proof of Eq. (17).

PHYSICAL REVIEW VOLUME 131, NUMBER 4 15 AUGUST 1963

Quasifree Proton-Neutron and Proton-Proton Scattering at 140 MeV*

J. LEFRANÇOIS,† R. A. HOFFMAN,‡ E. H. THORNDIKE,§ AND RICHARD WILSON
Cyclotron Laboratory, Harvard University, Cambridge, Massachusetts
(Received 27 March 1963)

Measurements of the neutron-proton triple scattering parameters R and A have been performed by scattering a polarized proton beam on a deuterium target. Quasifree proton-neutron events were separated by requiring a time coincidence between the scattered proton and the recoil neutron. The quasifree results were corrected by the method of Cromer and Thorndike (second following paper) to give the following equivalent free neutron-proton results:

$\theta_{c.m.}$	R	A
42°	+0.169±0.100	−0.020±0.089
52½°	+0.080±0.093	+0.070±0.074
63°	−0.023±0.073	+0.210±0.088
73½°	−0.151±0.095	+0.125±0.105
83½°	−0.146±0.210	+0.532±0.220

Measurements were also made requiring a coincidence between the scattered proton and a recoil proton. In this manner, the R and A parameters for quasifree proton-proton scattering in deuterium were obtained. The results are

$\theta_{c.m.}$	R	A
65½°	−0.246±0.061	−0.229±0.087
73½°	−0.273±0.064	−0.144±0.069
83½°	−0.050±0.125	+0.016±0.133

The free n-p values agree with the predictions of the Yale phase-shift solutions YLAN 3 and 3M. The quasifree p-p values agree with free p-p measurements.

I. INTRODUCTION

In recent years the proton-proton interaction has been studied with some vigor. Near 140 MeV, the cross section,[1] polarization,[1] and triple-scattering parameters[2–4] D, R, and A, have been measured. Similar programs have been carried out near 210 [5] and 315 MeV.[6] Phase-shift analyses performed on these measurements indicate that the p-p scattering matrix has been very nearly determined.[7]

* Supported by the joint program of the U. S. Office of Naval Research and the U. S. Atomic Energy Commission. A preliminary report on part of this work has been previously published [Phys. Rev. **125**, 973 (1962)]. The results quoted in the present article differ slightly from those in the preliminary report, and supercede them.

† Present address: Laboratoire des Hautes Energies, Orsay, France.

‡ Present address: Department of Physics, Union College, Schenectady, New York.

§ Present address: Department of Physics, University of Rochester, Rochester, New York.

[1] J. N. Palmieri, A. M. Cormack, N. F. Ramsey, and Richard Wilson, Ann. Phys. (N. Y.) **5**, 229 (1958).

[2] C. F. Hwang, T. R. Ophel, E. H. Thorndike, and Richard Wilson, Phys. Rev. **119**, 352 (1960).

[3] E. H. Thorndike, J. Lefrançois, and Richard Wilson, Phys. Rev. **120**, 1819 (1960).

[4] S. Hee and E. H. Thorndike (to be published).

[5] A. C. England, W. A. Gibson, K. Gotow, E. Heer, and J. Tinlot, Phys. Rev. **124**, 561; J. H. Tinlot and R. E. Warner, *ibid.* **124**, 890 (1961); K. Gotow, F. Lobkowicz, and E. Heer, *ibid.* **127**, 2206 (1962).

[6] J. E. Simmons, Phys. Rev. **104**, 416 (1956); O. Chamberlain, E. Segré, R. D. Tripp, C. Wiegand, and T. Ypsilantis, *ibid.* **105**, 288 (1957).

[7] G. Breit, M. H. Hull, Jr., K. E. Lassila, and K. D. Pyatt, Jr., Phys. Rev. **120**, 2227 (1960).